RSC Advances

PAPER

View Article Online
View Journal | View Issue

Cite this: *RSC Adv.*, 2021, **11**, 9395

Fe_2O_3 enhanced high-temperature arsenic resistance of CeO_2–La_2O_3/TiO_2 catalyst for selective catalytic reduction of NO_x with NH_3

Na Wang, *[a] Changfei Ye,[a] Huidong Xie,*[b] Chang Yang,[c] Jinhong Zhou[d] and Chengmin Ge[e]

Received 3rd January 2021
Accepted 8th February 2021

DOI: 10.1039/d1ra00031d

rsc.li/rsc-advances

High-temperature arsenic resistance catalysts of $CeLa_{0.5}Fe_x/Ti$ (x = 0, 0.1, 0.2, 0.3, 0.4, 0.5) series were prepared and measured under a simulation condition of arsenic poisoning. The as-prepared catalysts were characterized by XRD, SEM, TEM, and XPS. The specific surface area and pore size of the catalysts were measured. At x = 0.2, the catalyst shows the best arsenic resistance and catalytic performance. The active temperature range of the $CeLa_{0.5}Fe_{0.2}/Ti$ catalyst is 345–520 °C when the gas hourly space velocity is up to 225 000 mL g^{-1} h^{-1}. Compared with commercial vanadium-based catalysts, $CeLa_{0.5}Fe_{0.2}/Ti$ shows much better catalytic performance. The introduction of Fe will improve the dispersion of CeO_2 and increase the concentration of Ce^{3+} and unsaturated active oxygen on the surface. The NH_3-TPD and H_2-TPR results show that the $CeLa_{0.5}Fe_{0.2}/Ti$ catalyst has more acidic sites and more excellent redox performance than $CeLa_{0.5}Fe_0/Ti$. The $CeLa_{0.5}Fe_{0.2}/Ti$ catalyst might have application prospects in the field of selective catalytic reduction of NO_x with NH_3.

1. Introduction

Nitrogen oxides (NO_x) are some of the main pollutants in the atmosphere, which can do great harm to the ecological environment and human health, such as, acid rain, photochemical smog, ozone depletion, *etc.*[1] Selective catalytic reduction (SCR) of NO_x with ammonia is the most effective method to reduce NO_x in flue gas of stationary sources. Currently, the most widely used commercial SCR catalyst is V_2O_5–$WO_3(MoO_3)/TiO_2$.[2,3] The vanadium-based catalyst has many advantages as well as some unavoidable problems, such as, strong biological toxicity of vanadium, narrow temperature window (300–400 °C), easy oxidation of SO_2 to SO_3, and low N_2 selectivity at high temperature.[4] Recent reports have shown that CeO_2 is the most powerful substitute for V_2O_5 because of its non-toxicity, high reactivity, and excellent oxygen storage and release capabilities.[5–7] However, the adaptability and anti-inactivation ability of CeO_2 in a complicated flue gas environment is still an urgent problem to be solved. Heavy metal arsenic, often existing in the form of volatile As_2O_3 or As_2O_5 in high-temperature flue gas, is toxic to commercial SCR catalysts.[8] Early reports show that the arsenic poisoning of commercial catalysts is due to the coverage of the active sites on the surface of the catalyst by inactive As_2O_5 and the diffusion of arsenic oxides into the pores of the catalyst, which causes the blocking of the micropores in the catalysts.[9–11] The current widely accepted view is that chemical deactivation is the main reason, because arsenic of high oxidation state, As(v), can interact with the active site of vanadium to reduce the surface acid sites.[12–14] In order to improve the arsenic resistance, commercial vanadium-based catalysts often need many additives, such as WO_3 and MoO_3. It has been found that MoO_3 has better resistance to arsenic poisoning than WO_3 because MoO_3 can further improve the dispersion of active sites of vanadium.[15] Current literature on arsenic resistance mainly focuses on adding MoO_3 to commercial vanadium-based catalysts. However the highest NO conversion of these catalysts after arsenic poisoning is less than 80%.[16,17] It is also effective in improving the arsenic resistance of CeO_2-based catalysts by adding WO_3/MoO_3.[18–20] However the reported highest NO conversion of the CeO_2-based catalysts after arsenic poisoning is only 75%. So far, there is no report on the CeO_2-based catalyst by adding Fe_2O_3 as arsenic resistance catalyst. Recently, our research group has developed the CeO_2–La_2O_3/TiO_2 vanadium-free catalysts, which can be used at high temperature and are expected to replace commercial vanadium-based catalysts. Owing to its catalytic activity, sulfur resistance and porous properties, TiO_2 is an excellent catalytic carrier. La_2O_3 is a good auxiliary component for

[a]*College of Architecture and Civil Engineering, Xi'an University of Science and Technology, Xi'an, 710054, Shaanxi, China. E-mail: wangna811221@xust.edu.cn; Fax: +86-29-82202335; Tel: +86-29-82203378*

[b]*School of Chemistry and Chemical Engineering, Division of Laboratory and Equipment Management, Xi'an University of Architecture and Technology, Xi'an, 710055, Shaanxi, China. E-mail: xiehuidong@tsinghua.org.cn*

[c]*Division of Laboratory and Equipment Management, Xi'an University of Architecture and Technology, Xi'an, 710055, Shaanxi, China*

[d]*College of Geography and Environment, Baoji University of Arts and Sciences, Baoji, 721013, Shaanxi, China*

[e]*Shandong Dongyuan New Material Technology Co., Ltd, Dongying, 257300, Shandong, China*

active component of CeO_2 because of the formation of Ce–O–La bond on the surface of CeO_2, which increases the acidic sites of the catalyst and the adsorption of NH_3 and NO. Because Fe-based catalysts have good deNO_x performance[21,22] as well as good adsorption of arsenic owing to the formation of strong Fe–O–As chemical bond in the removal of the arsenic in the water treatment,[23–26] it is expected that Fe_2O_3 can be used as an arsenic resistance catalyst. In this paper, the Ce–La–Fe–Ti catalysts were obtained by an impregnation method, using anatase as the carrier and Ce–La–Fe oxides as the active component. The deNO_x activity of the as-prepared catalysts was measured. The as-prepared catalysts were characterized by XRD, SEM, TEM, and XPS. The reason for the arsenic resistance was discussed.

2. Experimental

2.1 Reagents and preparation

The Ce–La–Fe–Ti composite catalysts were prepared by an impregnation method. First, a certain volume of deionized water was added to a stainless steel reactor and heated to 60 °C. Then ammonia (25–28 wt%) and citric acid (analytical purity) were added to adjust the pH to 3–4 with stirring. After that, anatase pigment (TiO_2, industrial grade), $Ce(NO_3)_3\cdot 6H_2O$ (industrial grade), $La(NO_3)_3\cdot 6H_2O$ (industrial grade), and $(NH_4)_2Fe(SO_4)_2\cdot 6H_2O$ (analytical purity) were added according to the different weight ratios, $CeLa_{0.5}Fe_x/Ti$ ($x = 0$, 0.1, 0.2, 0.3, 0.4, 0.5), where 0.5 and x are the weight ratios of La (calculated as La_2O_3) and Fe (calculated as Fe_2O_3) to Ce (calculated as CeO_2). In all the Ce–La–Fe–Ti composite catalysts, the weight ratio of Ce–La–Fe to Ti (calculated as TiO_2) is 3 : 7. The suspension was stirred continuously for 2–3 h and evaporated by vacuum distillation for 1 h. Then the mixture was cooled to room temperature, ripen for 2 hours, dried at 105 °C for 12 h, and calcined at 500 °C in a muffle furnace for 5 h. Finally, the samples were used for the SCR activity test. For comparison, commercial vanadium-based catalysts obtained from the market were also used.

2.2 Catalyst activity tests

First, 1 g as-prepared catalysts were ground in a planetary ball mill for 90 min and soaked in 25 mL 1 mg mL^{-1} arsenic standard solution (calculated as As_2O_3) for 3 h to simulate its arsenic poisoning. The water solvent was completely evaporated, thus the loading amount of As_2O_3 on the catalyst was calculated to be about 2.5 wt%. Then the catalyst was adhered to an industrial honeycomb-shaped cordierite cylinder with size of $\varphi 20 \times L50$. After drying at 105 °C, the loaded cylinder was calcined in a closed tube furnace at 450 °C for 3 h. Then the loaded cylinder was put into a quartz tube furnace to test the activity of the catalyst. The loading amount of the catalyst is 0.8 g. The gas composition is 500 ppm NO, 500 ppm NH_3, 300 ppm SO_2, 3% O_2, 5% H_2O, and N_2 is used as the balance gas. The total gas flow is 3000 mL min^{-1}, hence the corresponding gas hourly space velocity (GHSV) is calculated to be 225 000 mL g^{-1} h^{-1}. The outlet gas concentrations of NO, NO_2, SO_2 were detected by the Germany Ecom flue gas analyzer and the N_2O concentration was detected by the KRM50 infrared flue gas analyzer. The temperature program was controlled by a computer. At each temperature, the experiment was kept for 30 min to stabilize before the data collection of the concentration of the outlet gas. The NO conversion and N_2 selectivity were calculated according to the formula (1) and (2).[27,28]

$$\text{NO conversion } (\%) = \frac{[\text{NO}]_{\text{in}} - [\text{NO}]_{\text{out}}}{[\text{NO}]_{\text{in}}} \times 100\% \quad (1)$$

$$\text{N}_2 \text{ selectivity } (\%) = \frac{[\text{NO}]_{\text{in}} - [\text{NH}_3]_{\text{in}} - [\text{NO}_2]_{\text{out}} - 2[\text{N}_2\text{O}]_{\text{out}} - [\text{NO}]_{\text{out}} - [\text{NH}_3]_{\text{out}}}{[\text{NO}]_{\text{in}} + [\text{NH}_3]_{\text{in}} - [\text{NO}]_{\text{out}} - [\text{NH}_3]_{\text{out}}} \times 100\% \quad (2)$$

2.3 Characterization

The Brunauer–Emmet–Teller (BET) specific surface area and pore volume of the samples were measured on the Micromeritics ASAP 2020 instrument. The morphology was observed on the Zeiss MERLIN compact field emission scanning electron microscope (FE-SEM) and a JEOL JEM 2100 plus transmission electron microscope (TEM). The X-ray diffraction (XRD) was performed on the Rigaku Ultima IV instrument, with a tube voltage of 40 kV, a tube current of 40 mA, and Cu Kα radiation. X-ray photoelectron spectroscopy (XPS) was performed on the Thermo ESCALAB 250XI electronic energy spectrometer, with C1s binding energy (284.8 eV) for energy calibration, X-ray source voltage of 16 kV, current of 14.9 mA, beam diameter of 650 μm. The temperature programmed chemical adsorption/reduction (TPD/TPR) was performed on the AutoChem1 II 2920 instrument. For NH_3-TPD, the catalyst was pre-treated under argon atmosphere at 350 °C for 1 h, then cooled down to 50 °C and adsorbed NH_3 to saturation. After that the temperature was raised to 100 °C and the catalyst was purged with Ar gas to desorb the physically adsorbed NH_3. Finally the temperature was raised to 500 °C at a ramping rate of 10 °C min^{-1} and the outlet NH_3 concentration was detected by the thermal conductivity detector (TCD). For H_2-TPR, the catalyst was pre-treated under Ar atmosphere at 350 °C for 1 h to remove the adsorbed gas on the surface, then cooled to room temperature. Then the catalyst was reduced in 10% H_2/Ar atmosphere from room temperature to 800 °C at a ramping rate of 10 °C min^{-1}. The H_2 consumption was detected by TCD.

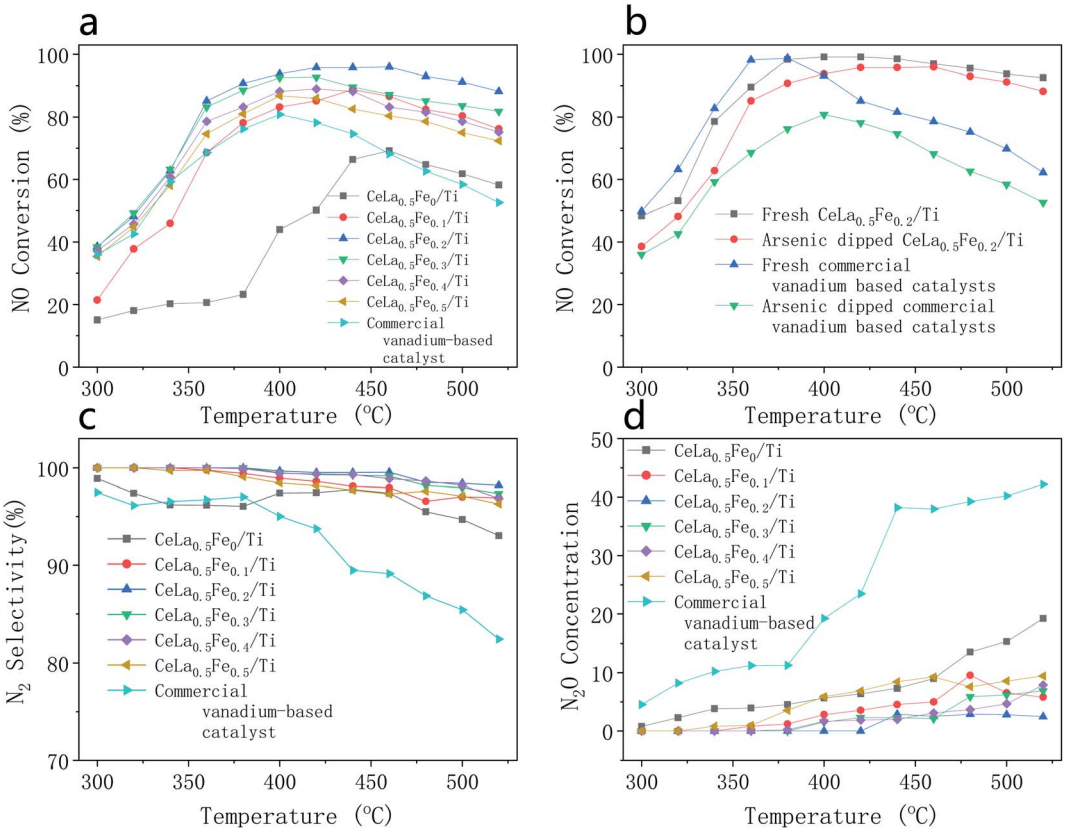

Fig. 1 Catalytic performance of catalysts with different components, all the catalysts were treated by arsenic as described in Section 2.2 except "Fresh" catalysts. (a) NO conversion of $CeLa_{0.5}Fe_x/Ti$ ($x = 0$, 0.1, 0.2, 0.3, 0.4, 0.5) and commercial vanadium-based catalysts; (b) NO conversion of $CeLa_{0.5}Fe_{0.2}/Ti$ and commercial vanadium-based catalyst with and without arsenic solution dipping; (c) N_2 selectivity of $CeLa_{0.5}Fe_x/Ti$ ($x = 0$, 0.1, 0.2, 0.3, 0.4, 0.5) and commercial vanadium-based catalyst; (d) N_2O concentration of $CeLa_{0.5}Fe_x/Ti$ ($x = 0$, 0.1, 0.2, 0.3, 0.4, 0.5) and commercial vanadium-based catalyst.

3. Results and discussion

3.1 Catalytic performance

Fig. 1 shows the catalytic performance of catalysts with different components, in which all the catalysts were treated by arsenic as described in Section 2.2 except "Fresh" catalysts. It can be seen from Fig. 1(a) that the loading of Fe_2O_3 greatly improves the NO conversion. As temperature increases, the NO conversion first increases and then decreases. Influenced by the kinetics reason, the NO conversion will increase whereas the increasing trend will decrease with the increase of the temperature. If the temperature is too high (>450 °C for $CeLa_{0.5}Fe_{0.2}/Ti$), the NO conversion will decrease due to the decrease of the N_2 selectivity. At the same temperature, the NO conversion first increases and then decreases with the increase of the Fe content. When the Fe_2O_3 content x is 0.2, the NO conversion of $CeLa_{0.5}Fe_x/Ti$ is the highest. The temperature range where the corresponding NO conversion is greater than 80% of $CeLa_{0.5}Fe_{0.2}/Ti$ is 345–520 °C. Commercial vanadium-based catalyst shows much weaker arsenic resistance than $CeLa_{0.5}Fe_{0.2}/Ti$. On the one hand, Fe-based catalysts have good $deNO_x$ performance,[4,5] on the other hand, Fe might form the bond of Fe–O–As[6–9] with As, which makes Fe preferentially combine with As to protect the main active site of CeO_2. However, excessive loading of Fe_2O_3 is detrimental to the $deNO_x$ performance of the catalyst, which can be attributed to the fact that excessive Fe_2O_3 will cover the active sites of the CeO_2 on the catalyst surface. Above 350 °C, the NO conversion of the catalyst is maintained at a high level, which may be related to the enhanced oxidation of CeO_2.[29] The introduction of La increases the surface unsaturated oxygen on the surface and the dispersibility of CeO_2.[30,31] From Fig. 1(b), it can be found that the commercial vanadium-based catalyst is significantly poisoned in arsenic environment, while $CeLa_{0.5}Fe_{0.2}/Ti$ catalyst is slightly affected in arsenic environment. The NO conversion of the $CeLa_{0.5}Fe_{0.2}/Ti$ is obviously better than commercial vanadium-based catalyst with regard to the arsenic resistance. In Fig. 1(c), the N_2 selectivity of the $CeLa_{0.5}Fe_x/Ti$ ($x = 0$, 0.1, 0.2, 0.3, 0.4, 0.5) catalysts is much better than that of commercial vanadium-based catalyst and $CeLa_{0.5}Fe_{0.2}/Ti$ shows the best N_2 selectivity (99.08–100%). In Fig. 1(d), the N_2O concentration of vanadium-based catalysts increases quickly whereas the N_2O concentrations of $CeLa_{0.5}Fe_x/Ti$ ($x = 0$, 0.1, 0.2, 0.3, 0.4, 0.5) increase slowly. This arsenic poisoning of vanadium-based catalysts is consistent with the results reported in the literature.[4]

3.2 XRD

Fig. 2 shows the XRD pattern of $CeLa_{0.5}Fe_x/Ti$ ($x = 0$, 0.1, 0.2) series. The main phase of the three catalysts is anatase TiO_2 (JCPDS no. 99-0008). The broad diffraction peaks indicate that

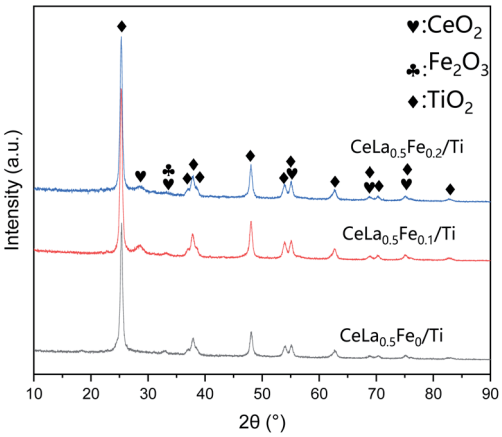

Fig. 2 XRD pattern of $CeLa_{0.5}Fe_x/Ti$ (x = 0, 0.1, 0.2) series.

the anatase is a nano-particle, which is consistent with the following SEM and TEM results. There are weaker cubic fluorite CeO_2 peaks (JCPDS no. 43-1002) near 28.6°, 33°, *etc.* The full width at half maximum (FWHM) of CeO_2 is wider than that of anatase, showing that the grain size of CeO_2 is much smaller than that of TiO_2. However, there is no phase related to the La_2O_3, indicating that La_2O_3 is highly dispersed on the catalyst surface in an amorphous state, which is similar to the literature.[32] The XRD peak of Fe_2O_3 (~33.15°, JCPDS no. 33-0664) is very weak and very wide, which indicates the Fe_2O_3 is amorphous. The FWHM of the (111) peak of the CeO_2 at 28.5° becomes wider with the increase of the Fe content, which means the addition of Fe decreases the CeO_2 grain size. Since CeO_2 is the main catalyst, small crystal size is beneficial to increase its catalytic activity. In addition, the peak of CeO_2 at 28.5° (after Gaussian fitting) moves towards higher angle direction, which might be caused by the formation of the solid solution of CeO_2–Fe_2O_3. This is because the radius of Ce^{4+} (eight-coordinated, 0.97 Å) is larger than that of Fe^{3+} (eight-coordinated, 0.78 Å). It is worth noting that although there are reports in the literature that anatase will transform into rutile at ~500 °C,[33] the rutile phase cannot be found in the catalysts, showing that the catalysts have good thermal stability.

3.3 SEM

Fig. 3 is the SEM images of the $CeLa_{0.5}Fe_x/Ti$ (x = 0, 0.1, 0.2) series. According to the reports, the catalysts with the size of nano-particles can show high catalytic activity.[34] As can be seen, the active components are highly dispersed on the surface of the

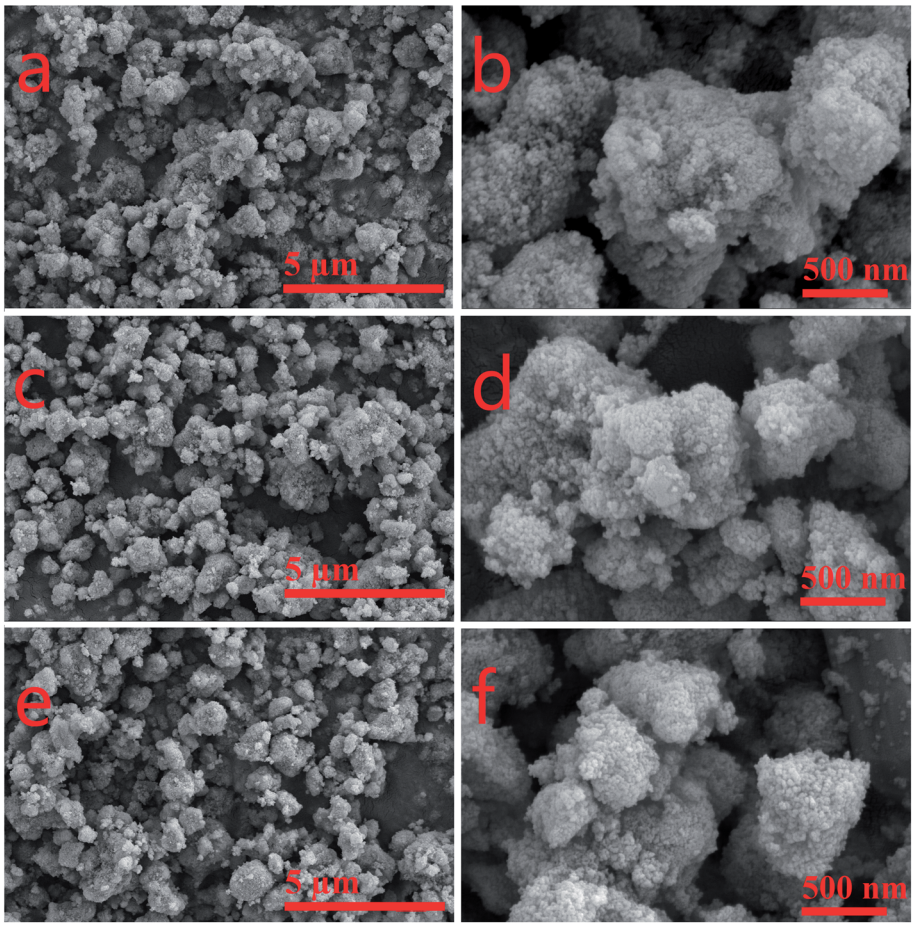

Fig. 3 SEM images of $CeLa_{0.5}Fe_x/Ti$ (x = 0, 0.1, 0.2) with different magnification. (a and b) $CeLa_{0.5}Fe_0/Ti$; (c and d) $CeLa_{0.5}Fe_{0.1}/Ti$; (e and f) $CeLa_{0.5}Fe_{0.2}/Ti$.

catalysts and the nano-particles form agglomerates with the size of sub-microns. The number of particles increases with the increase of the Fe content, which means that the addition of Fe may enhance the dispersion of CeO_2 on the surface of TiO_2. This is consistent with the XRD results.

3.4 TEM

Fig. 4 shows the TEM image, elemental mapping, and energy dispersive spectra (EDS) of $CeLa_{0.5}Fe_{0.2}/Ti$. The morphology in Fig. 4(a) clearly shows that the crystal size of the catalyst is tens of nanometers. In the HR-TEM image (Fig. 4(b)), the stripe spacing of 0.357 nm corresponds to the (101) plane of anatase TiO_2, and the stripe spacing about 0.318 nm corresponds to the (111) plane of CeO_2. The elemental mapping pictures of Ti, Ce, Fe, La, and O (Fig. 4(d–h)) show that the La, Ce, Fe and Ti elements are uniformly distributed in the catalysts. The EDS result in Fig. 4(i) shows that the main elements are Ti, La, Ce, Fe, and Cu, where Cu is caused by the Cu grid used to support the sample.

3.5 XPS

Fig. 5 is the XPS spectra of $CeLa_{0.5}Fe_x/Ti$ ($x = 0$, 0.1, 0.2). The peaks of Ce, La, Ti, Fe and C can be found in the survey spectra in Fig. 5(a). The Ce3d XPS spectra (Fig. 5(b)) can be fitted to nine peaks, named V_1 (≈880.7 eV), V_2 (≈882.3 eV), V_3 (≈885.8 eV), V_4 (≈888.6 eV), V_5 (≈898.3 eV), U_1 (≈900.8 eV), U_2 (≈903 eV), U_3 (≈907.3 eV), U_4 (≈916.7 eV). All V peaks correspond to $Ce3d_{5/2}$ spin orbits, and all U peaks correspond to $Ce3d_{3/2}$ spin orbits. The peaks of V_1, V_3, and U_2 correspond to Ce^{3+}, while the peaks of V_2, V_4, V_5, U_1, U_3, and U_4 correspond to Ce^{4+}.[35] From the peak area, the Ce^{3+} content on the CeO_2 surface increases significantly as the Fe content increases. Because of the different electrovalence of Fe^{3+} and Ce^{4+}, in order to maintain charge balance, the oxygen vacancy defects on the CeO_2 surface also increase as the Fe content increases, which are beneficial to the improvement of the catalytic activity.[36] The XPS of O1s (Fig. 5(c)) can be fitted into two peaks: O_α (surface unsaturated oxygen, ≈530.6 eV) and O_β (lattice oxygen, ≈528.7 eV). Calculated by the fitted peak area, the $O_\alpha/(O_\alpha + O_\beta)$ fractions of $CeLa_{0.5}Fe_0Ti$, $CeLa_{0.5}Fe_{0.1}Ti$, $CeLa_{0.5}Fe_{0.2}/Ti$ catalysts are 43.30%, 43.73% and 43.78%, respectively. Because the surface unsaturated oxygen O_α of CeO_2 has a higher mobility and a stronger catalytic performance than the lattice oxygen O_β, $CeLa_{0.5}Fe_{0.2}/Ti$ catalyst shows the best catalytic performance.[37] In Fig. 5(d), the peaks of Fe2p correspond to $Fe2p_{1/2}$ (724 eV),

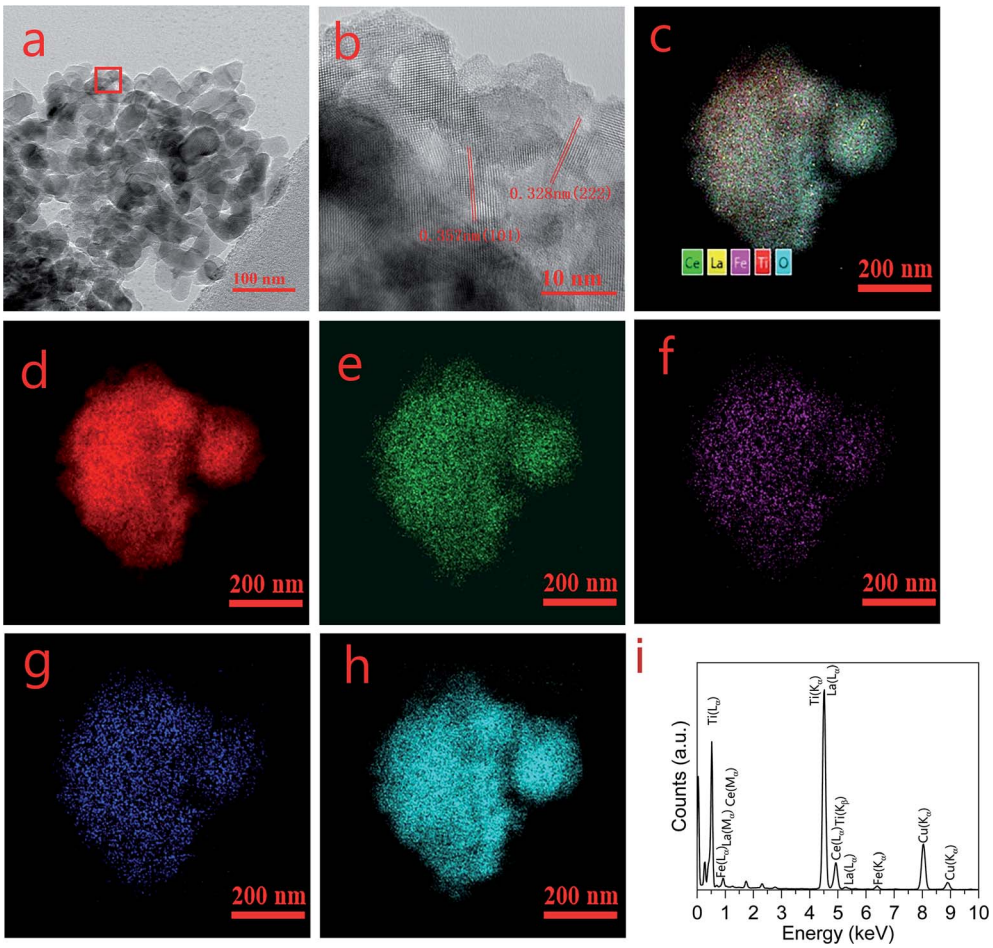

Fig. 4 TEM images, elemental mapping, and EDS of $CeLa_{0.5}Fe_{0.2}/Ti$. (a) TEM morphology, (b) HR-TEM, (c) all elements mapping, (d) Ti mapping, (e) Ce mapping, (f) Fe mapping, (g) La mapping, (h) O mapping. (i) EDS.

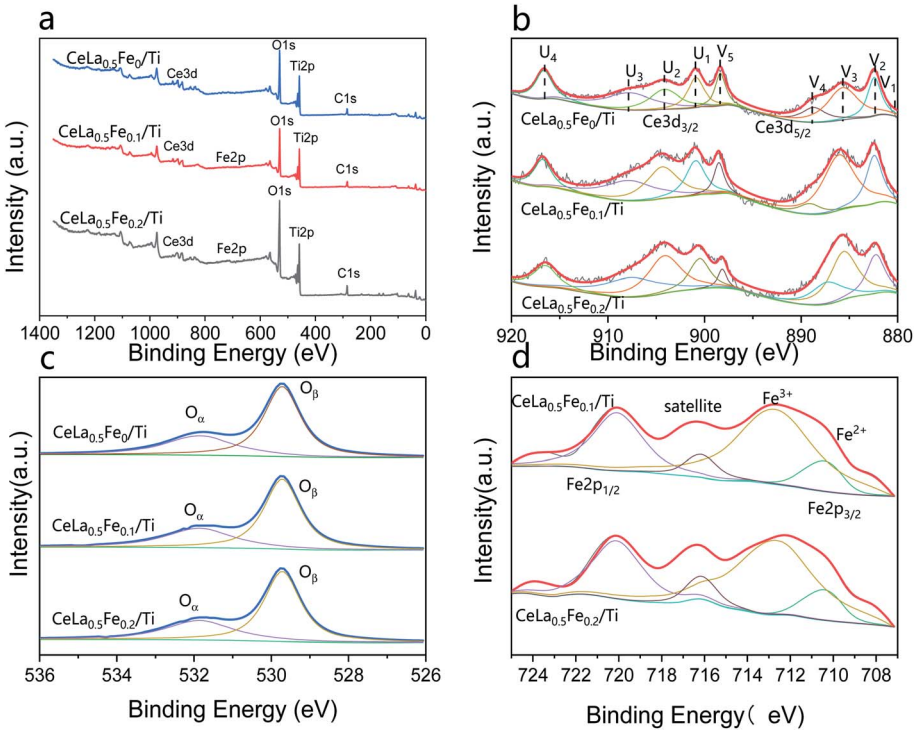

Fig. 5 XPS spectra of $CeLa_{0.5}Fe_x/Ti$ (x = 0, 0.1, 0.2). (a) Survey spectra; (b) Ce3d; (c) O1s; (d) Fe2p.

$Fe2p_{3/2}$ (711 eV) and satellite peaks. The peaks of $Fe2p_{3/2}$ are fitted by two peaks of Fe^{2+} (710.0 eV) and Fe^{3+} (712.8 eV).[38] The $CeLa_{0.5}Fe_{0.2}/Ti$ and $CeLa_{0.5}Fe_{0.1}/Ti$ catalysts have no obvious differences in shape and positions, showing that the valances of Fe in the two samples are the same or similar. No obvious satellite peak and asymmetric peak are observed at ~715 eV, and the peak positions of $2p_{3/2}$, satellite, and $2p_{1/2}$ are close to that of Fe^{3+}. However the existence of Fe^{2+} must be considered because Fe^{2+} can be fitted in the curve. Therefore, it can be concluded that Fe^{3+} is the major valence while Fe^{2+} is the minor valence on the surface.[39]

3.6 N_2 adsorption and desorption

The BET specific surface area, pore volume and pore diameter of $CeLa_{0.5}Fe_x/Ti$ (x = 0, 0.1, 0.2) series were measured by N_2 adsorption and desorption experiments. The results were shown in Table 1. Because the main components of the catalysts are TiO_2, CeO_2 and La_2O_3, and the content of Fe_2O_3 is very little, the change of Fe content has little effect on the specific surface area of the catalyst. The specific surface area increases and the pore size increases slightly. The reason may be that the introduction of Fe inhibits the growth rate of ceria grains and reduces the ceria grain size. This is consistent with the results of the XRD and SEM images.

Table 1 BET specific surface area, pore volume and pore diameter of $CeLa_{0.5}Fe_x/Ti$ (x = 0, 0.1, 0.2) series

Catalyst	S_{BET} ($m^2\ g^{-1}$)	V_p ($cm^3\ g^{-1}$)	D_p (nm)
$CeLa_{0.5}Fe_0/Ti$	78.1	0.040	3.25
$CeLa_{0.5}Fe_{0.1}/Ti$	79.7	0.039	3.28
$CeLa_{0.5}Fe_{0.2}/Ti$	79.9	0.041	3.32

3.7 NH_3-TPD and H_2-TPR

NH_3-TPD result reflects the acidity of the catalysts. Fig. 6(a) shows the NH_3-TPD curves of the $CeLa_{0.5}Fe_x/Ti$ (x = 0, 0.1, 0.2, 0.3) catalysts. As can be seen, the $CeLa_{0.5}Fe_0/Ti$ catalyst has two desorption peaks at about 350 °C and 290 °C. It is generally believed that the peak above 450 °C is related to the Lewis acid site (strong acid site) associated with the NH_3 molecule, and the peak near 300 °C is related to the Brønsted acid site (weak acid site) associated with NH_4^+ ions.[40] From the peak area, the quantity of the Brønsted acid sites on the surface of the catalyst increases with the increase of Fe content up to x = 0.2, which helps to increase the catalytic activity. This is consistent with the catalytic performance in Fig. 1.

H_2-TPR result reflects the redox characteristics of the catalysts. Fig. 6(b) shows the H_2-TPR curves of the $CeLa_{0.5}Fe_x/Ti$ (x = 0, 0.1, 0.2, 0.3) catalysts. The strong peaks of the four catalysts in the range of 450–580 °C correspond to the reduction process from Ce^{4+} to Ce^{3+}, which are closely related to the catalytic activity of the catalysts.[41] With the increase of Fe content x up to x = 0.2, the peak position shifts towards lower temperature direction from 577 °C to 473 °C, which means that the introduction of Fe makes the reduction of the surface oxygen on CeO_2 by H_2 more easy. However, when the Fe content increases to x = 0.3, the reduction peak changes from 473 °C to 515 °C, which means that the reduction of CeO_2 on the catalyst surface becomes more difficult. From the peak area, the H_2

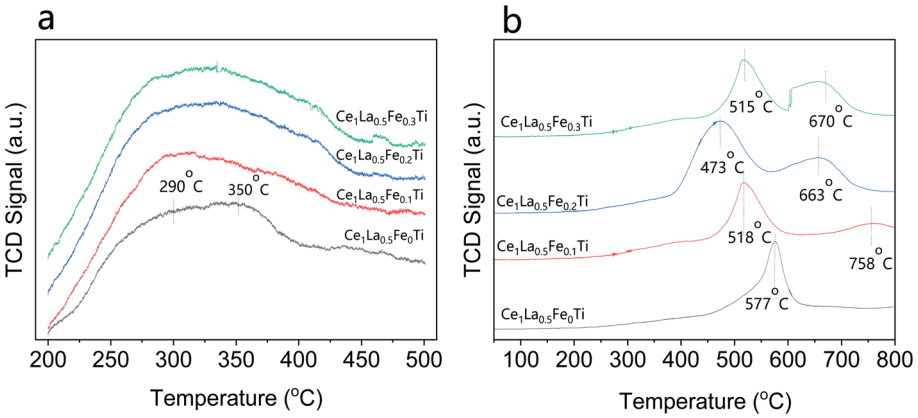

Fig. 6 (a) NH_3-TPD curves of the $CeLa_{0.5}Fe_x$/Ti ($x = 0$, 0.1, 0.2, 0.3) catalysts; (b) H_2-TPR curves of the $CeLa_{0.5}Fe_x$/Ti ($x = 0$, 0.1, 0.2, 0.3) catalysts.

consumption is $CeLa_{0.5}Fe_{0.2}$/Ti > $CeLa_{0.5}Fe_{0.3}$/Ti > $CeLa_{0.5}Fe_{0.1}$/Ti > $CeLa_{0.5}Fe_0$/Ti, showing that the surface oxygen on CeO_2 increases with the increase of Fe content, which is consistent with the XPS results. Based on the NH_3-TPD and H_2-TPR curves, it can be concluded that $CeLa_{0.5}Fe_{0.2}$/Ti catalyst has the most acidic sites and strongest redox performance.

4. Conclusions

An anti-arsenic SCR denitration catalyst with anatase as the carrier, CeO_2, as the main active components, and La_2O_3, Fe_2O_3 as the main auxiliary agent was prepared by the impregnation method. The optimized $CeLa_{0.5}Fe_{0.2}$/Ti catalyst exhibits better catalytic performance under arsenic environment than the commercial vanadium-based catalysts. After the introduction of the Fe_2O_3, the Ce^{3+} concentration, surface unsaturated oxygen, CeO_2 dispersibility, specific surface area, and acidic sites are all improved, which improves the catalytic activity in the arsenic environment. $CeLa_{0.5}Fe_{0.2}$/Ti catalyst has high NO conversion efficiency, excellent N_2 selectivity and arsenic resistance, which might be a candidate for SCR denitrification applications in the arsenic flue gas environment.

Conflicts of interest

There are no conflicts to declare.

Acknowledgements

The research was supported by the National Natural Science Foundation of China under grant no. 51708447, Key R&D Project of Shaanxi Province under grant no. 2019SF-250, and Major Scientific and Technological Innovation Projects of Shandong Province under grant no. 2019JZZY010343.

References

1 S. Luo, W. Zhou, A. Xie, F. Wu and T. Liu, Effect of MnO_2 polymorphs structure on the selective catalytic reduction of NO_x with NH_3 over TiO_2-palygorskite, *Chem. Eng. J.*, 2016, **286**, 291–299.

2 Z. Liu, J. Zhu, S. Zhang, L. Ma and S. I. Woo, Selective catalytic reduction of NO_x by NH_3 over MoO_3-promoted CeO_2/TiO_2 catalyst, *Catal. Commun.*, 2014, **46**, 90–93.

3 G. Busca, L. Lietti, G. Ramis and F. Berti, Chemical and mechanistic aspects of the selective catalytic reduction of NO_x by ammonia over oxide catalysts: A review, *Appl. Catal., B*, 1998, **18**, 1–36.

4 S. Brandenberger, O. Kröcher, A. Tissler and R. Althoff, The state of the art in selective catalytic reduction of NO_x by ammonia using metal-exchanged zeolite catalysts, *Catal. Rev.*, 2008, **50**, 492–531.

5 P. Li, Y. Xin, Q. Li, Z. Wang, Z. Zhang and L. Zheng, Ce–Ti amorphous oxides for selective catalytic reduction of NO with NH_3: Confirmation of Ce–O–Ti active sites, *Environ. Sci. Technol.*, 2012, **46**, 9600–9605.

6 R. Qu, X. Gao, K. Cen and J. Li, Relationship between structure and performance of a novel cerium-niobium binary oxide catalyst for selective catalytic reduction of NO with NH_3, *Appl. Catal., B*, 2013, **142**, 290–297.

7 H. Li, C. Y. Wu, Y. Li and J. Zhang, Superior activity of MnO_x CeO_2/TiO_2 catalyst for catalytic oxidation of elemental mercury at low flue gas temperatures, *Appl. Catal., B*, 2012, **111**, 381–388.

8 C. L. Senior, D. O. Lignell, A. F. Sarofim and A. Mehta, Modeling arsenic partitioning in coal-fired power plants, *Combust. Flame*, 2006, **147**, 209–221.

9 E. Hums, Is advanced SCR technology at a standstill? A provocation for the academic community and catalyst manufacturers, *Catal. Today*, 1998, **42**, 25–35.

10 Q. Lu, X. Q. Pei, Y. W. Wu, M. X. Xu, D. J. Liu and L. Zhao, Deactivation mechanism of the commercial V_2O_5–MoO_3/TiO_2 selective catalytic reduction catalyst by arsenic poisoning in coal-fired power plants, *Energy Fuels*, 2020, **34**, 4865–4873.

11 M. Kong, Q. C. Liu, X. Q. Wang, S. Ren, J. Yang, D. Zhao, W. C. Xi and L. Yao, Performance impact and poisoning mechanism of arsenic over commercial V_2O_5–WO_3/TiO_2 SCR catalyst, *Catal. Commun.*, 2015, **72**, 121–126.

12 F. Hilbrig, H. E. Göbel, H. Knözinger, H. Schmelz and B. Lengeler, Interaction of arsenious oxide with DeNox-catalysts: An X-ray absorption and diffuse reflectance infrared spectroscopy study, *J. Catal.*, 1991, **129**, 168–176.

13 S. Pritchard, S. Kaneko and K. Suyama, *Optimizing SCR catalyst design and performance for coal-fired boilers, EPA/EPRI 1995 Joint Symposium Stationary Combustion NOx Control*, May 16-19, 1995.

14 I. Morita, M. Hirano and B. H. K. K. Kure, *Development and commercial operating experience of SCR DeNOx catalysts for wet bottom coal fired boilers*, Power-Gen International, Dec 9–11, 1998.

15 E. Hums, A catalytically highly-active, arsenic oxide resistant V-Mo-O phase — results of studying intermediates of the deactivation process of V_2O_5 -MoO_3 -TiO_2 (anatase) $DeNO_x$ catalysts, *Res. Chem. Intermed.*, 1993, **19**, 419–441.

16 Y. Peng, W. Si, X. Li, J. Luo, J. Li, J. Crittenden and J. Hao, Comparison of MoO_3 and WO_3 on arsenic poisoning V_2O_5/TiO_2 catalyst: DRIFTS and DFT study, *Appl. Catal., B*, 2016, **181**, 692–698.

17 Y. Peng, J. Li, W. Si, J. Luo, Q. Dai, X. Luo, X. Liu and J. Hao, Insight into deactivation of commercial SCR catalyst by arsenic: An experiment and DFT study, *Environ. Sci. Technol.*, 2014, **48**, 13895–13900.

18 X. Li, J. Li, Y. Peng, X. Li, K. Li and J. Hao, Comparison of the structures and mechanism of arsenic deactivation of CeO_2–MoO_3 and CeO_2–WO_3 SCR Catalysts, *J. Phys. Chem. C*, 2016, **120**, 18005–18014.

19 X. Li, J. Li, Y. Peng, H. Chang, T. Zhang, S. Zhao, W. Si and J. Hao, Mechanism of arsenic poisoning on SCR catalyst of CeW/Ti and its novel efficient regeneration method with hydrogen, *Appl. Catal., B*, 2016, **184**, 246–257.

20 X. Li, X. Li, J. Li and J. Hao, Identification of the arsenic resistance on MoO_3 doped CeO_2/TiO_2 catalyst for selective catalytic reduction of NO_x with ammonia, *J. Hazard. Mater.*, 2016, **318**, 615–622.

21 G. H. Yao, K. T. Gui and F. Wang, Low-temperature de-NO_x by selective catalytic reduction based on iron-based catalysts, *Chem. Eng. Technol.*, 2010, **33**, 1093–1098.

22 M. Devadas, O. Kröcher, M. Elsener, A. Wokaun, G. Mitrikas, N. Söger, M. Pfeifer, Y. Demel and L. Mussmann, Characterization and catalytic investigation of Fe-ZSM5 for urea-SCR, *Catal. Today*, 2007, **119**, 137–144.

23 Z. C. Li, X. M. Liu, W. Jin, Q. S. Hu and Y. P. Zhao, Adsorption behavior of arsenicals on MIL-101(Fe): The role of arsenic chemical structures, *J. Colloid Interface Sci.*, 2019, **554**, 692–704.

24 M. A. V. Ramos, W. Yan, X. Li and B. Koel, Simultaneous oxidation and reduction of arsenic by zero-valent iron nanoparticles: understanding the significance of the coreshell structure, *J. Phys. Chem. C*, 2009, **113**, 14591–14594.

25 H. P. Feng, L. Tang, J. Tang, G. M. Zeng, H. Dong, Y. C. Deng, L. L. Wang, Y. N. Liu, X. Y. Ren and Y. Y. Zhou, Cu-doped Fe@Fe_2O_3 core-shell nanoparticle shifted oxygen reduction pathway for high-efficiency arsenic removal in smelting wastewater, *Environ. Sci.: Nano*, 2018, **5**, 1595–1607.

26 M. J. Uddin and Y. K. Jeong, Review: Efficiently performing periodic elements with modern adsorption technologies for arsenic removal, *Environ. Sci. Pollut. Res.*, 2020, **27**, 39888–39912.

27 Z. Liu, S. Zhang, J. Li and L. Ma, Promoting effect of MoO_3 on the NO_x reduction by NH_3 over CeO_2/TiO_2 catalyst studied with in situ DRIFTS, *Appl. Catal., B*, 2014, **144**, 90–95.

28 W. Shan, F. Liu, H. He, X. Shi and C. Zhang, A superior Ce-W-Ti mixed oxide catalyst for the selective catalytic reduction of NOx with NH_3, *Appl. Catal., B*, 2012, **115–116**, 100–106.

29 J. W. Shi, Y. Wang, R. B. Duan, C. Gao, B. R. Wang, C. He and C. M. Niu, The synergistic effects between Ce and Cu in $Cu_yCe_{1-y}W_5O_x$ catalysts for enhanced NH_3-SCR of NO_x and SO_2 tolerance, *Catal. Sci. Technol.*, 2019, **9**, 718–730.

30 B. Zhang, D. Li and X. Wang, Catalytic performance of La–Ce–O mixed oxide for combustion of methane, *Catal. Today*, 2010, **158**, 348–353.

31 Y. Dai, X. Y. Wang, D. Li and Q. G. Dai, Catalytic combustion of chlorobenzene over Mn-Ce-La-O mixed oxide catalysts, *J. Hazard. Mater.*, 2011, **188**, 132–139.

32 L. Gao, C. Li, P. Lu, J. Zhang, X. Du, S. Li, L. Tang, J. Chen and G. Zeng, Simultaneous removal of Hg^0 and NO from simulated flue gas over columnar activated coke granules loaded with La_2O_3-CeO_2 at low temperature, *Fuel*, 2018, **215**, 30–39.

33 O. Carp, C. L. Huisman and A. Reller, Photoinduced reactivity of titanium dioxide, *Prog. Solid State Chem.*, 2004, **32**, 33–177.

34 Z. Yan, J. Wang, R. Zou, L. Liu, Z. Zhang and X. Wang, Hydrothermal synthesis of CeO_2 nanoparticles on activated carbon with enhanced desulfurization activity, *Energy Fuels*, 2012, **26**, 5879–5886.

35 A. Gupta, M. Hegde, K. Priolkar, U. Waghmare, P. Sarode and S. Emura, Structural investigation of activated lattice oxygen in $Ce_{1-x}Sn_xO_2$ and $Ce_{1-x-y}Sn_xPd_yO_{2-\delta}$ by EXAFS and DFT calculation, *Chem. Mater.*, 2009, **21**, 5836–5847.

36 T. Montini, M. Melchionna, M. Monai and P. Fornasiero, Fundamentals and catalytic applications of CeO_2-based materials, *Chem. Rev.*, 2016, **116**, 5987–6041.

37 F. Liu, H. He, Y. Ding and C. Zhang, Effect of manganese substitution on the structure and activity of iron titanate catalyst for the selective catalytic reduction of NO with NH_3, *Appl. Catal., B*, 2009, **93**, 3760–3769.

38 Z. H. Chen, F. R. Wang, H. Li, Q. Yang and L. F. Wang, Low-temperature selective catalytic reduction of NO_x with NH_3 over Fe–Mn mixed-oxide catalysts containing $Fe_3Mn_3O_8$ phase, *Ind. Eng. Chem. Res.*, 2012, **51**, 202–212.

39 M. T. Van Dongen, D. Ng, L. V. Moura, D. Acharya, J. Wang, C. D. Easton, F. Wang and Z. Xie, Synthesis and characterisation of monolithic PTFE-modified MnO_x/FeO_x catalysts for selective catalytic reduction (SCR) of NO_x at low temperature, *J. Chem. Technol. Biotechnol.*, 2021, DOI: 10.1002/jctb.6612.

40 R. Zhang, W. Yang, N. Luo, P. Li, Z. Lei and B. Chen, Low-temperature NH_3-SCR of NO by lanthanum manganite perovskites: Effect of A-/B-site substitution and TiO_2/CeO_2 support, *Appl. Catal., B*, 2014, **146**, 94–104.

41 Z. Liu, J. Zhu, J. Li, L. Ma and S. I. Woo, Novel Mn-Ce-Ti mixed-oxide catalyst for the selective catalytic reduction of NO_x with NH_3, *ACS Appl. Mater. Interfaces*, 2016, **283**, 1044–1050.